J Fusion Energ (2012) 31:30–37
DOI 10.1007/s10894-011-9429-9

ORIGINAL RESEARCH

Correlations Among Neutron Yield and Dynamical Discharge Characteristics Obtained from Electrical Signals in a 400 J Plasma Focus

Felipe Veloso · Cristian Pavez · José Moreno · Victor Galaz · Marcelo Zambra · Leopoldo Soto

Published online: 20 May 2011

Abstract Dynamical discharge characteristics and their relation with the total neutron yield emitted from a 400 J plasma focus operating in deuterium gas are presented. The dynamical nature of the plasma focus is obtained merely from the analysis of the voltage and current electrical signals without considering any particular geometry for the plasma sheath. It is calculated that large neutron yields are obtained when plasma inductance, mechanical energy and plasma voltage at pinching time have larger values. In contrast, no correlations are found among neutron yields either with plasma propagation velocities or quantities at the beginning of the radial phase. There is also found that the current sheath geometry changes according to the gas pressure, having larger curvature for lower pressures. The calculations also provide estimations of sheath thicknesses at the detachment from the insulator in the range of 0.5–1 mm, being thicker for larger neutron yield.

Keywords Plasma focus · Compact devices · Neutron emission · Electrical diagnostics

F. Veloso (✉) · C. Pavez · J. Moreno · M. Zambra · L. Soto
Comisión Chilena de Energía Nuclear, Casilla 188-D, Santiago, Chile
e-mail: fveloso@cchen.cl; lsoto@cchen.cl

F. Veloso · C. Pavez · J. Moreno · V. Galaz · M. Zambra · L. Soto
Center for Research and Applications in Plasma Physics and Pulsed Power—P4, Casilla 188-D, Santiago, Chile

V. Galaz
Facultad de Ciencias Físicas y Matemáticas, Universidad de Chile, Av. Beauchef 850, Santiago, Chile

M. Zambra
Universidad Diego Portales, Santiago, Chile

Introduction

The plasma focus (PF) is a z-pinch type discharge, where an axial current flowing through a cylindrical plasma provides both energy input and magnetic field for its confinement. This pulsed plasma device has been widely studied in basic plasma physics and applied research related to X-ray, ions and neutrons sources (the latter, from D-D fusion reactions when operated on deuterium gas) [1]. In spite of many years of research, physical mechanism such as gas breakdown, hard X-ray emission and origin of fusion reactions (whether thermonuclear or beam target fusion) are still not fully understood or properly correlated with the different phases of the plasma focus. Several researches have been focused in the understanding of these processes, using different approaches both theoretical and experimental. Some scaling laws have been experimentally found [1–3], and they relate the measured neutron yield with the device energy and current. Besides, some efforts have been made in order to understand the similarities and differences on these devices [4]. There has been stated that the plasma foci are classified by its driver energy and the physical properties of the pinch plasma are similar among them.

In the past decades, the plasma focus research was made in devices operating with stored energies from 1 MJ to a few kJ on facilities having volumes of the order of tens cubic meter to a few cubic meter. However, in the last decade a new generation of fast and compact plasma focus devices has been developed [1, 5–25]. These devices operate with energy below 1 kJ and volumes less than a quarter of cubic meter, in the idea to produce portable sizes and reliable operation in repetitive mode. Several of these table top and miniaturized devices have been developed in our lab [5–12], extending the research in PF devices to

energies as low as 0.1 J [11, 12]. These kind of fast and compact devices have a shorter quarter of period and a smaller anode radius than devices working at energies greater than 1 kJ, thus the axial and the radial stages of the discharge, the duration of the pinch and the radiation pulses are shorter, and the source size of the radiation is smaller [12]. The spatial and temporal resolution of application of the radiations from conventional plasma focus could be improved using fast and compact plasma focus devices operating at energies lower than 1 kJ. Therefore, the study of all the phenomena related to breakdown, axial, radial and pinch phases and the correlations with the emitted radiations are very useful in this new generation of plasma focus devices.

In the PF discharges, the plasma is first generated around an insulator surface from the ionization of the background gas. Later, the resulting plasma sheath moves by the interaction between the current and its self-generated magnetic field. A z-pinch is formed when the plasma sheath coalesces at the symmetry axis of the configuration. The movement of this dynamical plasma sheath produces a time-varying plasma inductance, which is observed in the voltage and current measured in the experiments. On these experiments, the electrical signals (voltage and current derivative) are characterized by the appearance of a dip when the plasma reaches the central axis. This dip indicates the sudden increase of the plasma inductance due to plasma pinching. However, the information about the time variation of the plasma inductance is present on the entire duration of the electrical signals, and not only at the pinching time. This information can be extracted using circuit analysis where both generator and plasma are included. To compute the time varying inductance, the following equation is used [26]

$$L_p(t) = \frac{\int_{t_0}^{t} V(t)dt + \left(L_0^{'} + L_p(t_0)\right)I(t_0)}{I(t)} - L_0^{'} \qquad (1)$$

where $V(t)$ and $I(t)$ are the measured voltage and current, respectively; t_0 is the first peak on the dI/dt signal and corresponds to the time when the initial gas breakdown is complete and (1) can be applied. L_o' is the inductance from the plasma to the voltage probe connection. In order to get the inductance information, details on the processing method of the electrical signals can be found elsewhere [26, 27]. The validity of this model lies on two assumptions. First, the current flows on a single plasma sheath and the second assumption is that any resistance after $t = t_0$ is negligible when compared with inductive reactance. In the experiments described here, t_0 is on the order of 50 ns; and at this time both spark gap switch and plasma resistance are at least one order of magnitude lower than inductive reactance [26, 28]. A similar analysis of the electrical signals has been done in larger devices (18 kJ [27] and 5.7 kJ [29]), mainly concentrated in the energy transfer to the pinch plasma. This paper does not only provide analysis for a very low energy plasma focus (400 J), but also includes the dependence of the dynamical discharge characteristics (such as sheath formation and plasma movement prior to pinch) which are not present in these previous studies. All of this information is extracted from the electrical signals, without the use of additional time resolved diagnostic techniques, such as streak images, high speed cameras or magnetic probes. The dynamical characteristics are compared with the measured neutron yield under different operating pressures.

The Experiments

The experiments were carried out in the PF400 J [5] plasma focus (880 nF, 38 nH, 30 kV, 400 J) using deuterium as working gas. Electrode configuration consists in a 12 mm diameter central anode, partially covered by alumina on its basis. The anode has an effective length (i.e. not covered by the insulator) of 7 mm and a central hole of 3 mm radius. The cathode consists on a coaxial outer electrode of 26 mm diameter made of eight copper rods uniformly spaced and the discharge floor. Figure 1 shows a schematic diagram of the electrode geometry together with the equivalent circuit used for the analysis. In order to diagnose the discharge, current derivative and voltage were measured using properly calibrated Rogowski coil and fast resistive divider, both with response time lower than 5 ns. The experimental measurements on the calibration factors of the probes have shown that the measured values have errors lower than 2% each. The Rogowski coil is located in the return current path to the capacitors, and the resistive divider is connected to the anode $\sim$5 cm below the electrode arrangement shown in Fig. 1. The total neutron emission was measured using a silver activation counter calibrated with an Am–Be source. It was located 30 cm away from the discharge in the side-on direction. This neutron diagnostic technique provide total neutron yield with no temporal resolution. The dependance of the neutron yield as a function of deuterium pressure is also shown in Fig. 1. The characteristics of the device and its neutron emission as a function of pressure have been previously published in [5], but it does not include analysis on the dynamical behaviour of the discharge, which is the main scope of this paper. Besides, additional data and analysis about the neutron emission have been included.

The two values of inductance that should be calculated before the application of the algorithm are the plasma-to-resistive voltage divider connection ($L_0' = 9.5 \pm 0.2$ nH) and the initial plasma inductance ($L_p(t_0) = 1.2$ nH).

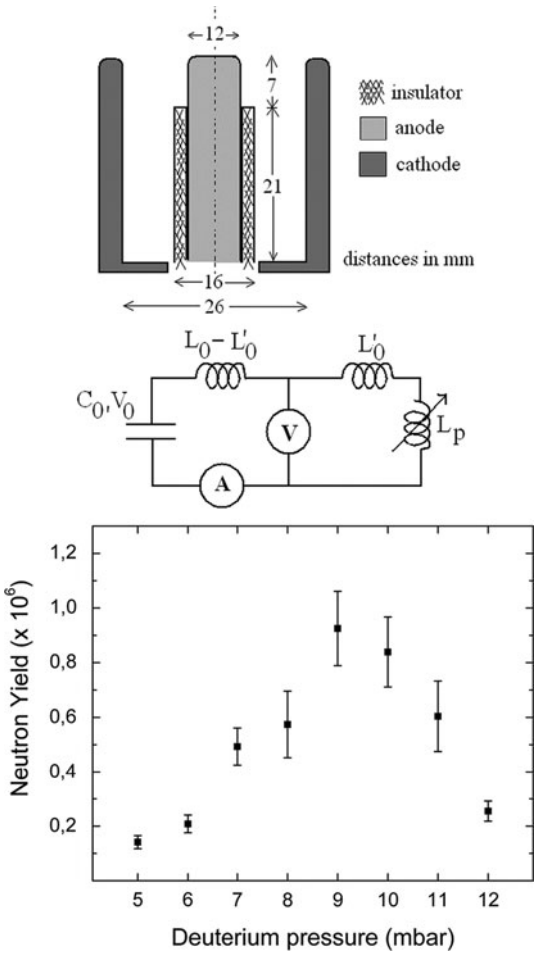

Fig. 1 (*top*) Schematic diagram of the PF-400 J together with its dimensions and the equivalent circuit used. (*bottom*) Measured neutron yield as function of pressure

These values were calculated using the method described in Ref. [26]. Figure 2 shows typical electrical signals from the experiment working in deuterium at 9 mbar. The current derivative and voltage are directly taken from the scope. Current trace was obtained by integration and the time varying inductance has been calculated using the algorithm previously described. From the inductance trace, four characteristics regions can be clearly identified: (1) very slow inductance increase, which states the current sheath formation over the insulator surface before its detachment from it at $t = t_d$, (2) nearly linear increase of the inductance, which is called 'axial phase' or 'run-down' phase, (3) sudden change in the inductance slope at a time $t = t_r$, which states the beginning of the radial phase and (4) inductance increase at a slower rate after the plasma pinching at $t = t_p$. This slower rate on the inductance trace means that the plasma is expanding and the pinch column is not radially compressing any longer. Regardless the operating conditions studied here, the observation of these four regions is clear in almost every shot. It should be mentioned that the definition of the pinching time t_p has been used as the time of the minimum of the dip on the current derivative trace, following previous studies on the field [21, 25, 30]. The main sources of systematic errors in the calculations are the calibrations factors of both resistive divider and Rogowski coil. The inductance trace shown in Fig. 2 includes error bars calculated with an error of 2% in both voltage and current probes. The average error in the calculated inductances is $\sim$0.4 nH for our device parameters. These error values do not greatly affect the general tendencies of the inductance trace previously mentioned, since they are related to the time history of the inductance and not to the inductance values themselves. This article reports the main characteristics of the first three regions and its relation with the total neutron yield. The error bars included on the plots are given by the standard error from the shot to shot fluctuation; with the exception of Fig. 2, where a single shot is shown and its associated error bars correspond to the probes calibration factors error

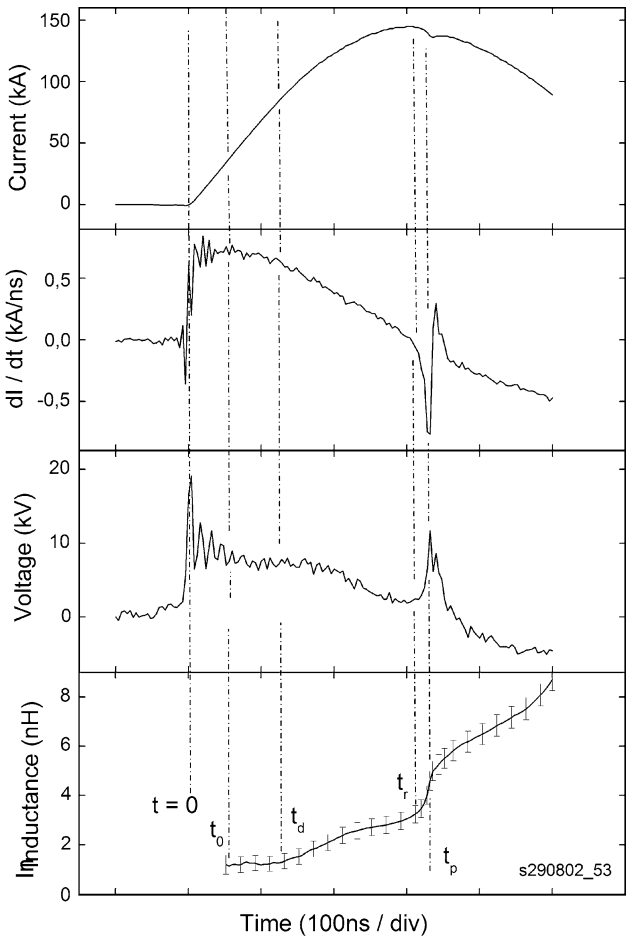

Fig. 2 Typical electrical signals of the PF-400 J. Vertical lines indicate the times t_0 (start time for the algorithm), t_d (detachment time), t_r (radial phase beginning) and t_p (pinching time)

propagation. Each value is an average of at least twelve shots under the same operating conditions.

As previously discussed, this model does not include resistance on the calculations. In order to compare the plasma inductance calculations with another model where the resistance is explicitly included, numerical simulations using the Lee model code [31, 32] were made. Briefly explaining, this numerical modeling adjusts the experimental current signal with a kinematic model of the current sheath by adjusting four dimensionless numerical parameters. This model, together with published data of the PF-400 J, was able to compute the experimentally measured neutron yield as function of pressure using a given set of parameters on the code [33]. Figure 3 shows the comparison of the inductance calculations using both the Lee model (with the parameters used in Ref. [33]) and the model described in "Introduction". Besides, the time derivative of the inductance (dL/dt) has also been calculated, since it behaves as 'dynamical resistance' on the circuit. In general, the Lee model provides highly valuable information regarding the plasma properties and its applicability on modeling our device has been demonstrated [33]. However, this model is not accurate on the initial inductance values since the insulator geometry in our experiment differs from the planar assumption of the simulation. The calculations presented in Fig. 3 show similar values for the time varying plasma inductance and also similar slopes during the radial phase. Additionally, the time derivatives of the inductances have also similar values. These calculations indicate consistency among the models and therefore, the results obtained from them should also be consistent.

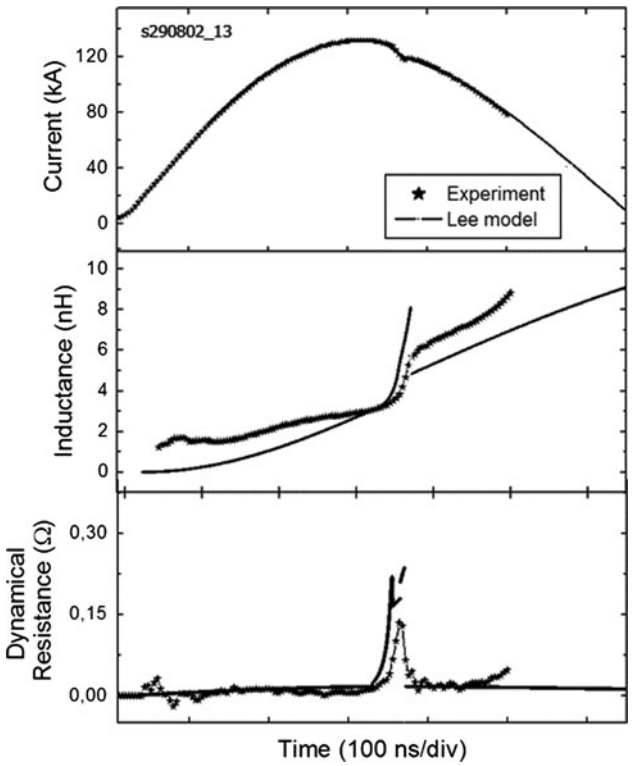

Fig. 3 Comparison among the model used in the paper (given by (1)) and the Lee model [31, 32] where resistivity is included

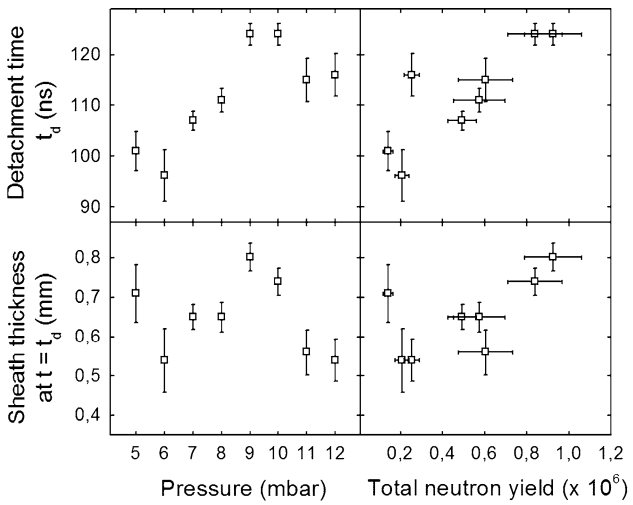

Fig. 4 Detachment time of the plasma sheath from the insulator. Sheath thickness estimations at this time is calculated from analytical models of ref [28]

Current Sheath Formation

The time varying inductance signals provide information about the plasma dynamics of the plasma focus, even though their calculations do not take into account either electrode geometry or operating condition. The first observed region is the very slow inductance increase (practically no variation on its value). During this time period, the plasma sheath stays attached over the insulator surface. Later on, this plasma sheath detaches from the insulator surface and starts moving axially toward the open end of the electrodes driven by the Lorentz force acting on it. Figure 4 shows the detachment time t_d as a function of pressure and neutron yield. Time references are relative to current start. The sheath attachment on the insulator surface can be easier to observe in this fast plasma focus in comparison with larger, microseconds plasma focus devices, since the average value of t_d is 110 ns, which represents $\sim$35% of the quarter period of the discharge. Besides, during this interval, the average plasma inductance is 1.39 nH, which is only $\sim$16% larger than the initial inductance (when the plasma sheath is confined to the insulator surface). It is possible to observe that t_d and the measured neutron yield show similar trend; i.e., maximum value at maximum emission. This might be explained for an

appropriate formation of the plasma layer before its lift off from the insulator surface. Then, the optimal neutron emission from our 400 J plasma focus seems to be influenced by this stage prior to the pinch. This observation has also been made by other researchers studying this phase using some different approaches [34, 35].

From the inductance values at the detachment time, the plasma sheath thicknesses are possible to estimate. The slow increase in inductance indicates the increase in thickness of the current conducting layer. Using this method, sheath thicknesses from 0.5 to 1 mm can be calculated. However, the systematic errors of the probes calibration factors previously discussed produce uncertainties on these values comparable to the values themselves. This fact does not allow the proper use of this method. In contrast, the detachment time t_d can be used instead, since its measurement is not affected by the errors of the electrical probes. Hence, the sheath thickness of the plasma layer can be estimated by considering available models of this initial phase in plasma focus. Some of these models are given in references [28, 36] where the ionization and lift off times have been analytically estimated. The ionization time is the time needed to complete the ionization in order to form a plasma sheath after the electrical breakdown of the background gas. The analytical estimation of this time is based on energy considerations. The lift off time is estimated considering that the main obstacle for the current sheath movement is its inertia [28]. The summation of these times is taken as the detachment time and numerical solutions for the sheath thicknesses are obtained. Using this method, the sheath thickness of the plasma at detachment from the insulator ranges from 0.5 to 0.8 mm. These values are similar to the obtained using geometrical estimations of the inductances at this time. Moreover, in this case the maximum sheath thickness is obtained at maximum neutron yield (i.e., at 9 mbar). These thicknesses estimations are shown in Fig. 4. In order to confirm these data, time resolved images are needed, but unfortunately no images of this stage on this energy range plasma focus (400 J) using deuterium are available. For the sake of comparison, Hassan et. al. [25] has reported similar detachment times using end-on images of the current sheath in a 100 J device operated in hydrogen. From these images, it is also possible to estimate sheath thicknesses lower than 2–3 mm; which is in accordance with our estimations based merely on the analysis of electrical signals.

Plasma at the Anode End

The calculation of the time varying inductance is also useful to calculate another valuable information, without being constricted to any specific plasma load geometry. It is known that the induced voltage on the load, and the mechanical energy of it is given by (2.1) and (3) [27, 29]

$$V_p(t) = \frac{d}{dt}\left(L_p I\right) \tag{2.1}$$

$$V_p(t = t_p) = V\left(t_p\right) - V(t_0) - \left(L_0' + 4.3nH\right)\left.\frac{dI}{dt}\right|_{t=tp} \tag{2.2}$$

$$E_m(t) = \frac{1}{2}\int_0^t \dot{L}_p I^2 dt \tag{3}$$

Equation 2.1 represents the plasma voltage at any time (without discounting the inductive drop on the electrode zone below the plasma sheath; where no plasma is present) and (2.2) is the plasma voltage at pinching time, which results from combining (1), (2.1) and the inductive voltage drop discount equivalent to the drop on the electrode geometrically calculated inductance. Figure 5 shows the inductance (L_p) and the mechanical energy (E_m) of the plasma at two different times: when the plasma starts its radial phase (t_r) and at the pinching time (t_p) as function of pressure and measured neutron yield. The plasma voltage at the pinching time (given by (2.2)) is also plotted in Fig. 5.

It is possible to observe that the plasma inductance decreases as the pressure increases at $t = t_r$ (i.e., at the end of the axial phase). As in this time, the plasma sheath has reached the top of the central electrode, this observation means that the plasma geometry is different for different

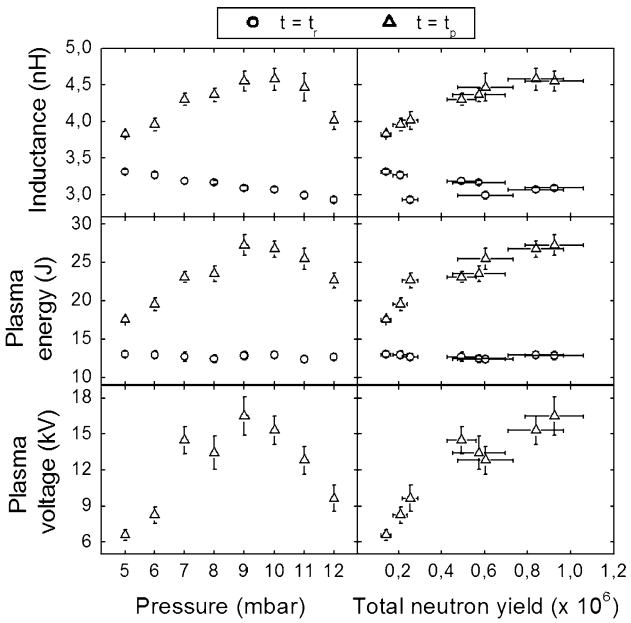

Fig. 5 Plasma voltage, mechanical energy and inductance as function of pressure and neutron yield. Circles correspond to the beginning of the radial phase ($t = t_r$) and triangles to the pinching time ($t = t_p$)

operating pressures. These differences should be related to the sheath curvature on each case, i.e. the curvatures are larger for lower pressures than those for higher pressures. This effect differs from the similar measurements made in a 5.7 kJ plasma focus, where their inductances at this time were rather invariant [29]. It is also possible to observe that the value of the inductance at this time is smaller than the expected value for a planar thin shell model of plasma sheath at the end of the axial phase (for our electrode geometry, the planar model inductance is 4.3 nH). This is coincident with similar measurements performed in the 5.7 kJ plasma focus of reference [29].

On the other hand, the mechanical energy of the plasma at $t = t_r$ is constant over the studied pressure range, and it represents $\sim$3.2% of the capacitor bank energy. It is interesting to point out that neither the mechanical energy nor the plasma inductance at the beginning of the radial phase are correlated to the final neutron emission. However, these tendencies change radically at the pinching time t_p. There are clear correlations among the inductance and the mechanical energy at this time with the neutron emission (high values provide high neutron yield). The maximum neutron yield is observed when $\sim$7% of the capacitor bank energy has been received by the plasma as mechanical energy. These energy calculations based on the experimental measurements show that the neutron yield is correlated with the work done by the plasma during the implosion (i.e., $E_m(t = t_p) - E_m(t = t_r)$). On the other hand, the plasma voltage also increases with the neutron yield, as both the mechanical energy and plasma inductance do. The plasma voltage at maximum neutron yield reaches $\sim$55% the charging voltage and it is 2.5 times larger than the voltage at minimum neutron yield.

At the end of the compression phase of the plasma towards the anode central axis, a characteristic dip is observed in the current derivative trace. It is known among experimental plasma focus physicists that the dip depth observed in the current derivative trace is related to proper operation of the plasma focus. There is a measurement of such observation in a 10 kJ plasma focus [37], but (as far as the authors aware) there are no measurements in very low energy devices operating with stored energy below 1 kJ. Figure 6 shows measurements of the dip in the current derivative trace against pressure and neutron yield. In these cases, the dip depth was measured from the current derivative trace original position (i.e., without dip) to the minimum measured value in the dip (as shown in Fig. 6). A clear correlation among dip depth and total neutron yield is observed. The deeper the dip is, the greater the neutron emission. The results obtained in this plasma focus of very low energy (400 J) agree with the observation on 10 kJ plasma focus and the usual belief on the operation of these kinds of devices.

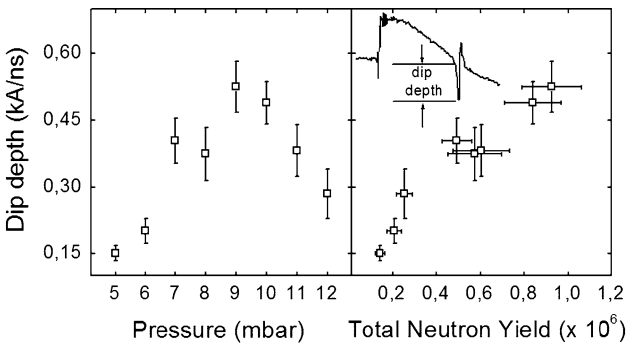

Fig. 6 Dip depth as function of pressure and neutron yield. A current derivative trace indicating the definition of the dip depth is included

Sheath Velocities Estimation

The velocity of the plasma sheath can be calculated from the inductance values, by assuming a particular geometry of the load. In order to avoid this kind of assumption, the values of the detachment, radial and pinching times (t_d, t_r and t_p respectively), together with the anode dimensions were used instead. The propagation velocities of the sheath are estimated by:

$$\langle vz \rangle = \frac{L_{\text{eff}}}{(t_r - t_d)} \tag{4}$$

$$\langle vr \rangle = \frac{a(1 - 0.12)}{(t_p - t_r)} \tag{5}$$

where $\langle vz \rangle$ and $\langle vr \rangle$ are the average axial and radial velocity estimations of the plasma sheath respectively, L_{eff} is the effective length of the anode and a is the anode radius. The radial velocity consider the movement of the plasma sheath up to a final radius of $0.12a$, according to the experimental measurements and scaling laws obtained for plasma focus devices [1, 4, 38]. Figure 7 shows average values of the radial and the axial velocities as a function of pressure and neutron yield. It can be observed that both estimated velocities decrease as the pressure increases, following a similar trend than the inductance at pinching time ($L_p(t = t_p)$). This is not a numerical similarity, since a physical origin can be ascribed to its explanation. It lies on the fact that the velocities shown here are time averaged while the inductances are instantaneous values. The explanation should be related to the accumulated mass by the plasma sheath during each phase, which increases with pressure. This mass accumulation results in a slower motion and smaller expansion of the plasma. Regarding the neutron yield, no correlations can be observed with the velocity estimations.

The average axial and radial velocities shown in Fig. 7 are consistent within the same order of magnitude and the correlation with pressure with the numerical simulations

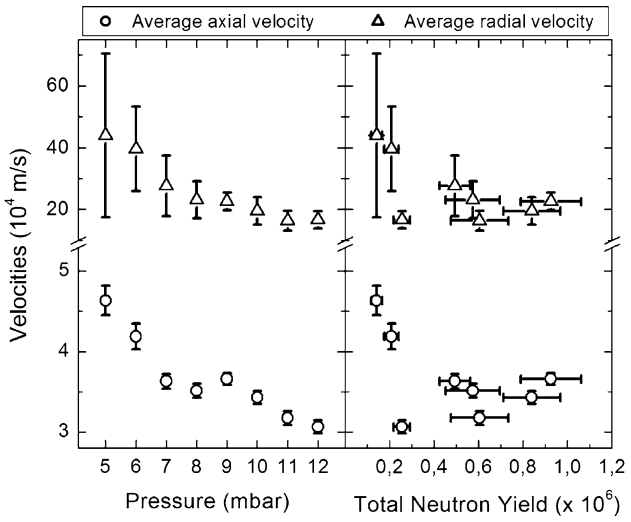

Fig. 7 Estimated axial (*circles*) and radial (*triangles*) velocities

using the Lee model code [31–33]. This confirms the consistency among both models discussed in "The Experiments". Further analyses on the accuracy of the estimated velocities among the models (which requires comparison with experimental measurements based on time-resolved images or similar diagnostics) are beyond the scope of this paper. The important point to emphasize is that the velocity estimation values show the same order of magnitude in both phases (axial and radial) and same trends with pressure. Additionally, these values are similar to experimental measurements made in the largest energy device (1 MJ plasma focus PF-1000) using time-resolved images [39], which reinforce the idea of scalability of plasma focus devices [4].

Discussion and Conclusions

Several characteristics of the discharge dynamics have been studied from the analysis of the electrical signals without considering any particular geometry for the plasma load. By measuring the voltage and the current derivative on the experiment, there was possible to obtain valuable information about the plasma sheath formation and dynamics before its final pinching onto the symmetry axis. This information has been compared with total neutron yield measurements performed with a silver activation counter and some physical quantities have been found to be related with the optimal neutron emission. Even though neutrons are emitted at the pinching time, the sheath detachment time from the insulator surface already shows similar trends with respect to pressure than neutron yield. This variation is ascribed to the increase in thickness of the plasma sheath. Sheath thicknesses are estimated in the range of 0.5–1 mm being thicker as larger the neutron yield is. After the detachment of this sheath, it travels with an average axial velocity of 3–5 $\times$ 10^4 m/s, showing no correlation with the neutron emission. When the plasma sheath gets the top of the anode, neither its mechanical energy nor the plasma inductance show similar trends with the neutron yield. Since in the previous phase (detachment) a correlation was found, the lost of it should indicate that the differences in the geometrical shape of the plasma sheath (as discussed on "Plasma at the Anode End") have more influence on the inductance calculation than the differences in sheath thickness. Additionally, no correlations are found among plasma sheath velocities and neutron yield.

Later on, when the plasma pinches on axis both mechanical energy and plasma voltage increase as neutron yield increases. Since thermonuclear fusion could be related to higher mechanical energy (due to its relation with plasma temperature at pinching), and beam target mechanism to higher plasma voltages (due to their relation with deuterons acceleration); it is not possible from the analysis of the electrical signals to differentiate which fusion mechanism is predominant and probably both mechanisms are improved under optimal operating conditions.

The analysis of the electrical signals has demonstrated to be a useful tool for future comparison of different plasma focus, since the method is not constrained to any particular geometry or operating condition. The dynamical characteristics presented here correspond to a very low energy device (400 J plasma focus), but some of these observations are common with large energy devices. Dip depth correlation with the neutron yield and sheath velocities are common features on plasma focus devices regardless their stored energy in the capacitor bank. The correlations found in this very low energy device indicate that the neutron emission is influenced by the early phases of the discharge and the optimization on the performance of the plasma focus should include an appropriate study of them.

Acknowledgments This work is supported by the Chile Bicentennial Program in Science and Technology grant ACT 26, Center for Research and Applications in Plasma Physics and Pulsed Power Technology (P4 Project) F Veloso is supported by CCHEN and grant PSD-01, PBCT. The authors acknowledge to Dr. P Silva his contribution during data acquisition and the fruitful discussions with Drs. A Clausse, H Bruzzone and H Acuña.

References

1. L. Soto, Plasma Phys. Control. Fusion **47**, A361 (2005)
2. G. Decker, H. Flemming, J. Kaeppeler, T. Oppenlander, G. Prob, P. Schilling, H. Schmidt, M. Shakhatre, M. Trunk, Plasma Phys. **22**, 245 (1980)
3. J. Pouzo, M. Milanese, IEEE Trans. Plasma Sci. **31**, 1237 (2003)
4. L. Soto, C. Pavez, A. Tarifeño, J. Moreno, F. Veloso, Plasma Sour. Sci. Technol. **19**, 055017 (2010)

5. P. Silva, J. Moreno, L. Soto, L. Birstein, R.E. Mayer, W. Kies, Appl. Phys. Lett. **83**, 3269 (2003)
6. L. Soto, A. Esaulov, J. Moreno, P. Silva, G. Sylvester, M. Zambra, A. Nazarenko, A. Clausse, Phys. Plasmas **8**, 2572 (2001)
7. P. Silva, L. Soto, J. Moreno, G. Sylvester, M. Zambra, L. Altamirano, H. Bruzzone, A. Clausse, C. Moreno, Rev. Sci. Instrum. **73**, 2583 (2002)
8. J. Moreno, P. Silva, L. Soto, Plasma Sour. Sci. Technol. **12**, 39 (2003)
9. P. Silva, L. Soto, W. Kies, J. Moreno, Plasma Sour. Sci. Technol. **13**, 329 (2004)
10. L. Soto, P. Silva, J. Moreno, M. Zambra, W. Kies, R.E. Mayer, A. Clausse, L. Altamirano, C. Pavez, L. Huerta, J.Phys. D: Appl. Phys. **41**, 205215 (2008)
11. L. Soto, C. Pavez, J. Moreno, M. Barbaglia, A. Clausse, Plasma Sour. Sci. Technol. **18**, 015007 (2009)
12. C. Pavez, L. Soto, IEEE Trans. Plasma Sci. **38**, 1132 (2010)
13. A.V. Dubrovsky, V.A. Gribkov, Y.P. Ivanov, P. Lee, S. Lee, M. Liu, V.A. Samarin, Nukleonika **46**(Suppl 1), S107–S111 (2001)
14. R. Verma, R.S. Rawat, P. Lee, M. Krishnan, S.V. Springham, T.L. Tan, IEEE Trans. Plasma Sci. **38**, 652 (2010)
15. M. Barbaglia, H. Bruzzone, H. Acuña, L. Soto, A. Clausse, Plasma Phys. Control. Fusion **51**, 045001 (2009)
16. M. Milanese, R. Moroso, J. Pouzo, Eur. Phys. J. D **27**, 77 (2003)
17. R.K. Rout, P. Mishra, A.M. Rawool, L.V. Kulkarni, S.C. Gupta, J. Phys. D Appl. Phys. **41**, 205211 (2008)
18. R. Shukla, S.K. Sharma, P. Banerjee, R. Das, P. Deb, T. Prabahar, B.K. Das, B. Adhikary, A. Shyam, Rev. Sci. Instrum. **81**, 083501 (2010)
19. R. Verma, R.S. Rawat, P. Lee, S.V. Springham, T.L. Tan, M. Krishnan, J. Phys. D Appl. Phys. **42**, 235203 (2009)
20. R. Verma, R.S. Rawat, P. Lee, M. Krishnan, S.V. Springham, T.L. Tan, Plasma Phys. Control. Fusion **51**, 075008 (2009)
21. R. Verma, R.S. Rawat, P. Lee, S. Lee, S.V. Springham, T.L. Tan, M. Krishnan, Phys. Lett. A **373**, 2568–2571 (2009)
22. R. Verma, R.S. Rawat, P. Lee, S.V. Springham, T.L. Tan, M.V. Roshan, M. Krishnan, J. Plasma Fusion Res Ser. **8**, 1283 ((2009))
23. R. Verma, P. Lee, S. Lee, S.V. Springham, T.L. Tan, R.S. Rawat, M. Krishnan, Appl. Phys. Lett. **93**, 101501 (2008)
24. R. Verma, M.V. Roshan, F. Malik, P. Lee, S. Lee, S.V. Springham, T.L. Tan, M. Krishnan, R.S. Rawat, Plasma Sour. Sci. Technol. **17**, 045020 (2008)
25. S.M. Hassan, T. Zhang, A. Patran, R.S. Rawat, S.V. Springham, T.L. Tan, D. Wong, W. Wang, S. Lee, V.A. Gribkov, S.R. Mohanty, P. Lee, Plasma Sour. Sci. Technol. **15**, 614 (2006)
26. H. Bruzzone, H. Acuña, M. Barbaglia, A. Clausse, Plasma Phys. Control. Fusion **48**, 609 (2006)
27. J.W. Mather, P.J. Bottoms, Phys. Fluids **11**, 611 (1967)
28. H. Bruzzone, R. Vieytes, Plasma Phys. Control. Fusion **35**, 1745 (1993)
29. H. Bruzzone, H. Acuña, A. Clausse, Brazilian J Phys **38**, 117 (2008)
30. F. Castillo Mejia, M. Milanese, R. Moroso, J. Pouzo, J. Phys. D Appl. Phys. **30**, 1499 ((1997))
31. S. Lee, in *Radiations in Plasmas*, vol. II ed. by B.E. McNamara (World Scientific, Singapore, 1984), pp. 978–987
32. S. Lee,in *Radiative Dense Plasma Focus Computational Package*: RADPF, 2010 http://www.intimal.edu.my/school/fas/UFLF/; http://www.plasmafocus.net/IPFS/modelpackage/File1RADPF.htm
33. S. Lee, S.H. Saw, L. Soto, S.V. Springham, S.P. Moo, Plasma Phys. Control. Fusion **51**, 075006 (2009)
34. W. Kies, Plasma Phys. Control. Fusion **28**, 1645 (1986)
35. M. Zakaullah, A. Waheed, S. Ahmad, S. Zeb, S. Hussain, Plasma Sour. Sci. Technol. **12**, 443 (2003)
36. H. Bruzzone, H. Acuña, A. Clausse, Plasma Phys. Control. Fusion **49**, 105 (2007)
37. D.A. Freiwald, K.R. Prestwich, G.W. Kuswa, E.H. Beckner, Phys. Lett. A **36**, 297 (1971)
38. S. Lee, A. Serban, IEEE Trans. Plasma Sci. **24**, 1101 (1996)
39. M. Scholz, R. Miklaszewski, M. Paduch, M. Sadowski, A. Szydlowski, K. Tomaszewski, IEEE Trans. Plasma Sci. **30**, 476 (2002)